Interferometer within a molecule

B. M. Garraway and S. Stenholm
Research Institute for Theoretical Physics, University of Helsinki, Siltavuorenpenger 20 C, SF-00170 Helsinki, Finland
(Received 21 January 1992)

We show how interferometry can be carried out within a molecule. The method can be used to test semiclassical quantum mechanics and to map out Born-Oppenheimer energy surfaces. The interference occurs between molecular wave packets that travel through different molecular states. Packet splitting and recombination is carried out at laser-induced level crossings. We have compared the exact quantum-mechanical behavior (calculated numerically on a Cray computer) with a pseudoclassical method.

PACS number(s): 34.50.Rk, 03.65.−w, 82.30.−b, 42.50.−p

I. INTRODUCTION

In quantum mechanics, every time a final state can be reached classically through two different pathways, an interference term appears from the two contributions. In optics, this is the manifestation of the wave nature of light which has been utilized in many ways for beam manipulations and precision measurements. With particles, the electron microscope and neutron diffractometer are based on the corresponding quantum effect. Only recently has it become possible to observe interference with atomic particles scattered from strong radiation or material structures; for an up to date review of the situation see Ref. [1].

In this paper we are going to look at another interferometric effect occurring inside a molecule excited in a time-dependent way. Using femtosecond-long laser pulses, it has now become possible to excite well-defined molecular states and to study their evolution in real time [2]. By the use of additional lasers, one can mix the wave packet with other levels in a controlled way, and redistribute the original excitation on sets of levels with different spatial dependence. If the wave packets are able to recombine, they will display quantum-mechanical interference which carries information about the history of both components of the mixture. Thus we have created a matter interferometer inside the molecule.

In chemical physics various coherent methods have been suggested for the steering of molecular reactions. For a survey of these suggestions, see the publication [3] and references therein. That work presents an experiment involving the interference between wave packets, but in contradistinction to our work it treats wave packets moving on a single excited electronic energy surface. Their interference derives from the time difference between their coherent excitation, and hence the setup is analogous to a Ramsey fringe experiment instead of a separated-path interferometer.

We illustrate the operation of a simple molecular interferometer in Fig. 1(a). This shows two Born-Oppenheimer potential functions depending on the one-dimensional nuclear coordinate X. We assume that the initial wave packet ψ_{I} is excited to the potential surface 2 at the position X_0. It starts to move down the potential slope, but soon encounters and interacts with another level 1, which is coupled to level 2 by a laser in resonance with 1 and 2 at X_a and also at X_b. Between these places the state consists of a linear superposition of the two wave packets ψ_{II} and ψ_{III} which propagate independently until the second crossing at X_b. Here there is a coherent remixing of the packets, which have acquired different phases in traveling from X_a to X_b. In Fig. 1(a) we see that part of ψ_{II} is mixed with ψ_{III} through photoabsorption to form ψ_{V}. And likewise, part of ψ_{III} is mixed with ψ_{II} through a stimulated-emission process to form ψ_{IV}. The mixing process is coherent and we shall see that it adds its own phase shifts. These shifts, together with the difference in phase accumulated between X_a and X_b, re-

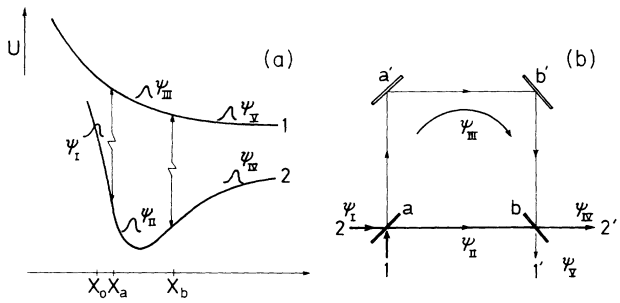

FIG. 1. (a) This figure shows the level scheme of the interferometer. The two coupled levels are labeled 1 and 2. The initial packet ψ_{I} travels on level 2 until it encounters the resonance position with the laser at X_a. It is then split into ψ_{II} and ψ_{III} which propagate independently to the second crossing at X_b where the recombination takes place and the interference is produced. The outputs are taken at ψ_{IV} and ψ_{V}. (b) An optical analog of the wave-mechanical interferometer. Optical input is at 1 or 2 corresponding to input at level 1 or level 2. The light is split at the partially silvered mirror a and travels through two different paths. The path lengths may be varied by moving the mirror pair a'-b'. The light is recombined at the mirror b and the output taken from 1′ or 2′.

sult in interference and fringes. A slight change in phase can dramatically alter the yield [$|\psi_{IV}|^2$ or $|\psi_V|^2$ in Fig. 1(a)] on levels 1 or 2 at a detection point well beyond the crossings. This is the physical model to be discussed in the rest of the paper.

To illuminate the operation of our molecular system as an interferometer, we show its optical analogue in Fig. 1(b). The incoming light signal ψ_I enters the beam splitter a and is divided into two paths as ψ_{II} and ψ_{III}. These go through the system in different ways and are recombined at the splitter b into the signal ψ_{IV} which shows interference depending on the phases acquired along the two paths. The signal ψ_V arises in a similar fashion.

The optical interferometer can be operated in a pulsed manner as our molecular system, but it is usually used in the steady state. The theoretical treatment is then carried out using the optical modes of the system, which include the appropriate splitting and remixing of the signals. In our molecular case, we introduce a similar steady-state description in terms of constant-energy eigenmodes of the potential configuration combined with an equivalent particle ensemble. Treating this in a semiclassical way we develop an analytic description which can be compared with the exact quantum-mechanical results obtained numerically from a Cray computer. The theoretical treatment consists in part of an *ad hoc* approach which is justified by its consequences.

In Sec. II we define the details of the molecular system described above and give an example of the quantum-mechanical motion of a packet. Then in Sec. III we develop an analytic description based on an equivalent particle ensemble and time-independent wave functions. In Sec. IV we compare the results from theory with the exact numerical results and find that they agree surprisingly well. Finally, Sec. V summarizes our results, discusses the application of the interferometer, and suggests some extensions and improvements.

II. THE MODEL

At the beginning of the experiment a molecular wave packet is created at the position X_0 on level 2. We have already discussed how such packets may be created and modeled in Ref. [4]. The packet is initially stationary on the level 2 and it will accelerate downwards until it is close to X_a where it is affected by the laser and distributed between the two levels. Stimulated processes may transfer the packet upwards to level 1, preserving its coherence. The amount of transfer depends on the way the energy difference between the two levels changes as well as the intensity of the laser. So by varying the parameters one can achieve any distribution of the state between the two levels. The particular form of the potentials is not too important in this paper though for numerical convenience we will use Morse potentials or similar exponential functions. We have chosen the upper surface 1 shown in Fig. 1(a) to be of a dissociating type and the lower surface 2 may contain some bound states. We will denote the spatial dependence on energy by the potentials as $\mathcal{U}_1(X)$ and $\mathcal{U}_2(X)$.

At the end of the experiment the final detection can be carried out in many ways. There may be fluorescence from one of the levels, or a photoabsorption measurement can be made. If the final state is a dissociating one, then the final products may have signatures in their spectroscopy. If the dissociating products are ions then the final detection is even easier. The same kind of detection can be used in conjunction with the field-ionization technique.

As we discussed in Refs. [5,6], when there is resonance between the Born-Oppenheimer levels and the laser we can model the situation with a system of crossing energy levels that are "dressed" with the laser photons. That is, if we shift the level 2 up by a single photon's energy we obtain level crossings at X_a and X_b as shown in Fig. 2. In the rotating-wave approximation the wave packet obeys a set of coupled Schrödinger equations on the two levels [5,6]:

$$\begin{aligned} i\hbar\frac{\partial}{\partial T}\Psi_1(X,T) &= \left\{-\frac{\hbar^2}{2m}\frac{\partial^2}{\partial X^2}+\mathcal{U}_1(X)\right\}\Psi_1(X,T) \\ &\quad +\mathcal{V}\Psi_2(X,T)\ , \\ i\hbar\frac{\partial}{\partial T}\Psi_2(X,T) &= \left\{-\frac{\hbar^2}{2m}\frac{\partial^2}{\partial X^2}+\mathcal{U}_2(X)+\hbar\omega\right\}\Psi_2(X,T) \\ &\quad +\mathcal{V}\Psi_1(X,T)\ . \end{aligned} \tag{1}$$

The functions Ψ_1 and Ψ_2 are the wave-function components that propagate on the two levels. The components are coupled by $\mathcal{V}$ which represents the time-independent interaction of the laser. The energy of a laser photon is $\hbar\omega$ and this is the shift of level 2 that creates the crossings. For numerical convenience we rescale these equations by factors T_s and X_s related by

$$T_s = 2mX_s^2/\hbar \tag{2}$$

and we introduce the parameters

$$t = T/T_s,\quad x = X/X_s,\quad x_0 = X_0/X_s,\quad x_a = X_a/X_s,\ \ldots\ . \tag{3}$$

With the definition of the scaled coupling, and scaled and shifted potentials,

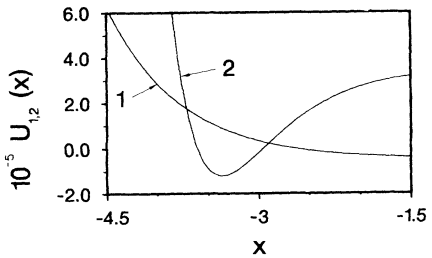

FIG. 2. This shows the shifted levels producing laser-induced crossings. The following parameters define the potentials as given in Eq. (6) and are the same in all the following figures: $A_1=1245.0$, $a_1=1.4$, $B_1=3.0\times10^5$, $A_2=60.0$, $a_2=2.9$, $B_2=-1800.0$, and $b_2=2.0$. All these parameters are in the scaled units of Eq. (2). Specifically to this figure, we have $\Delta=7.0\times10^5$. Adjusting the value of Δ will move the levels closer together or further apart.

$$V \equiv \frac{2mX_s^2}{\hbar^2}\mathcal{V} ,$$
$$U_1(x) \equiv \frac{2mX_s^2}{\hbar^2}\mathcal{U}_1(X_s x) , \tag{4}$$
$$U_2(x) \equiv \frac{2mX_s^2}{\hbar^2}\mathcal{U}_2(X_s x) + \omega T_s ,$$

we find the scaled equations

$$i\frac{\partial}{\partial t}\Psi_1(x,t) = \left\{-\frac{\partial^2}{\partial x^2} + U_1(x)\right\}\Psi_1(x,t) + V\Psi_2(x,t) ,$$
$$i\frac{\partial}{\partial t}\Psi_2(x,t) = \left\{-\frac{\partial^2}{\partial x^2} + U_2(x)\right\}\Psi_2(x,t) + V\Psi_1(x,t) . \tag{5}$$

We have solved these equations by a numerical method outlined in Ref. [4] which preserves the full quantum-mechanical behavior of the wave functions. An example of the wave-packet motion is given in Figs. 3(a) and 3(b) where we plot $P_1 = |\Psi_1(x,t)|^2$ and $P_2 = |\Psi_2(x,t)|^2$ as a function of both x and t. The initial packet is a Gaussian function of width $\sigma_0 = 0.01$ in scaled units. The positions of the crossings are marked by the thin time-independent lines on the surface. It is seen that the packets both disappear and appear in the region of these crossings. The potentials used in these calculations have been chosen to have the form (as illustrated in Fig. 2)

$$U_1(x) = A_1 e^{-a_1 x} + B_1 - \Delta/2 ,$$
$$U_2(x) = A_2 e^{-a_2 x} + B_2 e^{-b_2 x} + \Delta/2 , \tag{6}$$

where B_1 is a shift factor (determined by the molecular structure) and Δ is a detuning factor that determines the position of the two levels with respect to each other. Changing the frequency of the laser effectively changes the value of Δ. We have chosen A_1, A_2, B_2, a_1, a_2, and b_2 to be constants.

The initial packet is seen in Fig. 3(a). As it accelerates to the first crossing it rapidly loses height. This is partly because of the shape of the potential it moves in. Like a narrow packet in a harmonic oscillator, it gets wider as it moves down into the potential well. However, the well is not harmonic; there is dispersion and the initial packet never recovers. It loses height also because its probability is being transferred to the level 2, as may be seen in Fig. 3(b). This transfer is possible only near the crossings where the difference in energy between U_1 and U_2 is comparable to the coupling V.

After the first crossing, some Rabi flopping may be clearly seen due to the coherence between the two packets on different surfaces. These oscillations rapidly wash out because of both dispersion and the energy difference as the packets leave the crossing region. Between the crossings the packets propagate independently until they arrive at the second crossing. In this example, the packet on level 1 arrives first, and mostly disappears to level 2 [Fig. 3(b)] leaving only a trail of bumps. The main part of the packet from level 2 arrives later and forms the major part of the final probability.

This interferometer differs from usual devices in that it operates in a pulsed mode; we have packets propagating through the system. Thus if the time difference is too great in traveling along the two paths, the final packets may separate and we then lose the interference effect. That is, we do not have a single packet ψ_{IV} or ψ_{V} in Fig. 1(a), but pairs of spatially separated packets as almost seems the case in Fig. 3. Any phase difference between the packets would lose significance when they are well separated. It would still be possible to make simple semiclassical predictions by adding the probabilities of packet pairs separately. However, the case of partially overlapping packets is beyond such a simple approach. In the next section we will see how we can overcome this by a pseudoclassical model which at its heart *always* retains the interference effect.

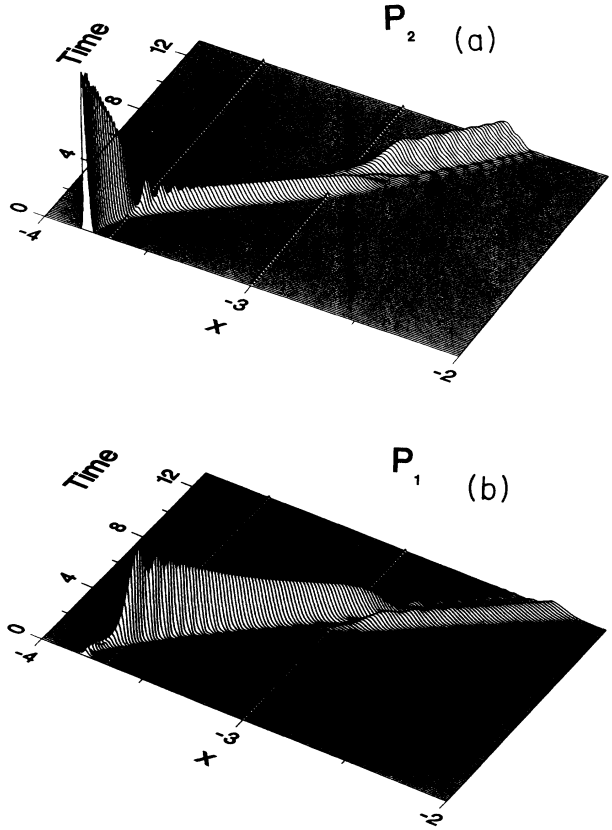

FIG. 3. This figure shows the wave-packet motion on the two levels as a function x and t. The probability density $P_2(x,t)$ is plotted in (a) and $P_1(x,t)$ is shown in (b). The initial position of the wave packet is $x_0 = -3.79$, its width is $\sigma_0 = 0.01$, and the coupling is $V = 2.0 \times 10^4$. Other parameters are the same as in Fig. 2.

III. A PSEUDOCLASSICAL MODEL

Because the main observable in our system is a phase difference, no model based on a purely classical propagation can give the right result. In this section we will combine an approach based on particle propagation and semiclassical wave functions to calculate the observable entity in our molecular interferometer.

We start by exciting a localized wave packet from some unspecified ground state to level 2. When the exciting pulse is short enough, we showed in Ref. [4], that the shape of the ground state is faithfully reproduced on the excited level, which is taken to be a Born-Oppenheimer state of the molecule. In the same work, we argued that many features of the quantum description can be reproduced by splitting up the original wave function into an equivalent ensemble of classical particles with a probability distribution $|a_2(x_i)|^2$ corresponding to the spatial density of the ground-state wave function at point x_i. If we assume the ground-state potential to be (approximately) harmonic, we may use

$$a_2(x_i)=(2\pi\sigma_0^2)^{-1/4}\exp\left\{-\frac{(x_i-x_0)^2}{4\sigma_0^2}\right\} . \tag{7}$$

This wave packet which is transferred to level 2 has zero initial velocity. Equation (7) will be valid over a finite interval; parts of the initial wave function outside this are assumed to have a negligible effect on the outcome of the experiment. The coefficients $a_2(x_i)$ will be used below to give the probability of finding the energy of the particle, E_i, in a unique way. We assume the corresponding particle of the equivalent ensemble to propagate through the potential configuration without interference from particles with other energies. The individual particles excited at x_i with zero velocity will have the total energy

$$E_i \equiv U_2(x_i) . \tag{8}$$

We treat the future fate of this particle in a time-independent way analogous to that used in scattering theory.

The states of the system in the basis of the Born-Oppenheimer levels will be written as vectors

$$\Psi(x)=\begin{bmatrix}\psi_1(x)\\ \psi_2(x)\end{bmatrix} , \tag{9}$$

which we also write as

$$\Psi(x)=\psi_1(x)\hat{\mathbf{e}}_1+\psi_2(x)\hat{\mathbf{e}}_2 , \tag{10}$$

where

$$\hat{\mathbf{e}}_1=\begin{bmatrix}1\\0\end{bmatrix} \quad \text{and} \quad \hat{\mathbf{e}}_2=\begin{bmatrix}0\\1\end{bmatrix} . \tag{11}$$

As the probability of excitation of the particle at $x=x_i$ is unity, we impose the boundary condition

$$\Psi(x=x_i)=\begin{bmatrix}0\\1\end{bmatrix}=\hat{\mathbf{e}}_2 . \tag{12}$$

This boundary condition will be imposed on the solution of the full coupled eigenvalue problem,

$$\left[-\mathbf{I}\frac{\partial^2}{\partial x^2}+\mathbf{U}(x)\right]\Psi^E(x)=E\Psi^E(x) , \tag{13}$$

where $\mathbf{I}$ is the unit matrix and we have introduced the potential matrix

$$\mathbf{U}(x)=\begin{bmatrix}U_1(x) & V\\ V & U_2(x)\end{bmatrix} . \tag{14}$$

The energy eigenvalue E is a parameter that will be followed through the calculation.

If we now observe some property of the wave function at a position beyond the second crossing, $x_f > x_b$, we find a probability amplitude

$$\Psi^E(x_f)=\mathbf{G}(x_f,x_i|E)\Psi^E(x_i) . \tag{15}$$

To obtain the propagator $\mathbf{G}$, we should solve Eq. (13).

When we calculate $\mathbf{G}(x_f,x_i|E^i)$ we have to include the effect of the coupling V. We do this in two ways: first we carry out an adiabatic diagonalization of the potential matrix, to obtain the approximate eigenstates. These should be a good approximation away from the level crossings. Then to include the effect of the crossings, we use a Landau-Zener matching of the wave functions coming into, and going out of, the crossing regions. To the extent that the potentials can be linearized near the crossings, this is an exact result.

We start by a local unitary transformation

$$\mathbf{W}(x)=\begin{bmatrix}\cos\theta/2 & -\sin\theta/2\\ \sin\theta/2 & \cos\theta/2\end{bmatrix} \tag{16}$$

of the states to

$$\Phi(x)=\mathbf{W}(x)\Psi(x) . \tag{17}$$

If we choose the angle θ according to

$$\tan\theta(x)=-2V/\Delta U(x) , \tag{18}$$

with

$$\Delta U(x)=U_1(x)-U_2(x) \tag{19}$$

we will be able to diagonalize $\mathbf{U}$ and we find that Eq. (13) becomes

$$\left[-\mathbf{I}\frac{\partial^2}{\partial x^2}-2\gamma\frac{\partial}{\partial x}+\tilde{\mathbf{U}}(x)\right]\Phi(x)=E\Phi(x) , \tag{20}$$

where we have a velocity-dependent coupling

$$\gamma(x)=\begin{bmatrix}0 & \theta'/2\\ -\theta'/2 & 0\end{bmatrix} , \tag{21}$$

and the new potential matrix

$$\tilde{\mathbf{U}}(x)=\begin{bmatrix}\mathcal{E}_+ +(\theta'/2)^2 & -\theta''/2\\ \theta''/2 & \mathcal{E}_- +(\theta'/2)^2\end{bmatrix} . \tag{22}$$

The adiabatic potential curves are now given by

$$\mathcal{E}_\pm(x)=[U_1(x)+U_2(x)]/2\pm[\Delta U(x)^2/4+V^2]^{1/2} . \tag{23}$$

In the following we adopt an adiabatic approximation, i.e., we assume the angle θ to depend on x slowly enough that we can neglect all derivatives of θ. This decouples the two components of Eq. (20) allowing us to write down the eigenfunctions $\phi_\pm^E(x)$ as the eigenfunctions of the separate potentials $\mathcal{E}_\pm(x)$. As seen from Eq. (18) this

procedure cannot hold near the level crossings. That is why we need the Landau-Zener approach to match the states across these.

In the region where the adiabatic approximation holds we may use the WKB wave functions in the form

$$\phi_\alpha^{\mathrm{WKB}}(x,E)=\frac{1}{[k_\alpha(x)]^{1/2}}\exp\left\{i\int_{x_a}^{x}k_\alpha(x')dx'\right\}, \tag{24}$$

where we have introduced

$$k_\alpha(x)=[E-\mathcal{E}_\alpha(x)]^{1/2}, \tag{25}$$

with α denoting the adiabatic levels ($\alpha=\pm$). In this way the functions $\phi_\alpha^{\mathrm{WKB}}(x,E)$ constitute the components of an approximation to the $\mathbf{\Phi}^E(x)$ eigenfunctions, which in turn determine $\mathbf{\Psi}^E(x)$. We have chosen to refer the phase factor of $\phi_\alpha^{\mathrm{WKB}}$ to the crossing point x_a, where it is taken to be zero. The change of phase between the crossings can accordingly be expressed in terms of the adiabatic states by the matrix

$$\mathbf{S}^E(x_b,x_a)=\begin{bmatrix}\exp\{i\Phi_+^E(x_b,x_a)\} & 0\\ 0 & \exp\{i\Phi_-^E(x_b,x_a)\}\end{bmatrix}, \tag{26}$$

where

$$\Phi_\alpha^E(x,x_a)=\int_{x_a}^{x_b}dx'[E-\mathcal{E}_\alpha(x')]^{1/2}. \tag{27}$$

Consideration of the normalization factor in Eq. (24) is not needed. The matrix $\mathbf{S}^E$ will apply to all wave functions $\phi_\alpha^E(x)$ once the value of E is given. We note that we define the WKB wave functions in terms of the adiabatic eigenstates.

In order to account for the transfer of the wave function across the crossing at x_a (and subsequently x_b), we introduce the explicitly time-dependent Landau-Zener problem [7] in the bare basis (level 1 and level 2),

$$i\frac{\partial}{\partial t}\begin{bmatrix}c_1(t)\\ c_2(t)\end{bmatrix}=\begin{bmatrix}\lambda_a u_a t & V\\ V & -\lambda_a u_a t\end{bmatrix}\begin{bmatrix}c_1(t)\\ c_2(t)\end{bmatrix}. \tag{28}$$

Here the potential slope is linearized and taken as

$$\lambda_a=\frac{1}{2}\frac{\partial}{\partial x}\Delta U(x)\bigg|_{x=x_a} \tag{29}$$

with the velocity u_a of the equivalent particle entering the crossing. This velocity is found without ambiguity in the bare basis as $u_a=2[E-U_{1,2}(x_a)]^{1/2}$ in scaled units. [At the crossing, by definition, $U_1(x_a)=U_2(x_a)$.] In [6] we showed that this gives a good agreement between wave-packet calculations and Landau-Zener computations.

The coupling interchanges the bare levels between incoming and outgoing states, and hence it follows that we may write the transfer matrix across the crossing in terms of the dressed levels as

$$\begin{bmatrix}c_2(\infty)\\ c_1(\infty)\end{bmatrix}=\mathbf{T}_a^E\begin{bmatrix}c_1(-\infty)\\ c_2(-\infty)\end{bmatrix}. \tag{30}$$

The Landau-Zener calculation [8] gives exactly the transfer matrix

$$\mathbf{T}_a^E=\begin{bmatrix}-\sqrt{1-P}\,e^{i\xi} & \sqrt{P}\\ \sqrt{P} & \sqrt{1-P}\,e^{-i\xi}\end{bmatrix}, \tag{31}$$

where the transfer probability

$$P=\exp(-\pi\Lambda), \tag{32}$$

and the phase

$$\xi=-\frac{\pi}{4}+\frac{\Lambda}{2}\ln\left[\frac{\Lambda}{2}\right]-\frac{\Lambda}{2}-\arg\left[\Gamma\left[\frac{\Lambda}{2}\right]\right], \tag{33}$$

are given in terms of the adiabaticity parameter

$$\Lambda=\frac{V^2}{|\lambda_a u_a|}. \tag{34}$$

When this is large, the adiabatic mixing of levels is nearly complete. The transfer matrix $\mathbf{T}_a^E$ is used to match the adiabatic wave functions in the regions $x<x_a$ to those at $x>x_a$. The index E indicates the dependence on the energy.

At the crossing x_b we make a second Landau-Zener calculation to obtain $\mathbf{T}_b^E$. This uses λ_b defined as in Eq. (29) except that the derivative is evaluated at $x=x_b$. Likewise the velocity u_b is calculated as $u_b=2[E-U_{1,2}(x_b)]^{1/2}$.

All the phase mixing occurs from just before x_a to just after x_b, and consequently we can now write, from Eqs. (15), (26), and (31),

$$\mathbf{G}(x_b,x_a|E)=\mathbf{T}_b^E\mathbf{S}^E(x_b,x_a)\mathbf{T}_a^E. \tag{35}$$

Because both the initial-state preparation and the detection couple to the bare states we need the matrix (35) in the representation of the states as defined by the basis Eq. (11). Thus we introduce

$$G_{jk}(E)=\langle\hat{\mathbf{e}}_j\mathbf{T}_b^E\mathbf{S}^E(x_b,x_a)\mathbf{T}_a^E\hat{\mathbf{e}}_k\rangle \tag{36}$$

which determines the scattering from input k to output j at the energy E.

However, the initial state is not prepared at $x=-\infty$, but at x_i where the effect of the coupling between the levels is already felt. In Eqs. (31) and (36) we have obtained $\mathbf{G}$ in terms of the adiabatic states ϕ_α^E, and hence we need to evaluate the incoming state [defined in Eq. (12) at $x=x_i$] in terms of these. Using the transformation (16) we find that

$$\mathbf{\Phi}(x=x_i)=\mathbf{W}(x_i)\begin{bmatrix}0\\ 1\end{bmatrix}=\begin{bmatrix}-\sin\theta(x_i)/2\\ \cos\theta(x_i)/2\end{bmatrix}. \tag{37}$$

The particle is created with probability unity on the bare level 2 and at the position $x=x_i$ with zero velocity. This probability is divided between the two adiabatic states in such a way that both energy and momentum are conserved. This follows if the components are both given

zero velocity and the energies $\mathcal{E}_{\pm}(x_i)$ defined by Eq. (23). As Eq. (37) determines their relative probabilities, we find that the average energy is conserved;

$$\mathcal{E}_{-}(x_i)\cos^2[\theta(x_i)/2]+\mathcal{E}_{+}(x_i)\sin^2[\theta(x_i)/2] = U_2(x_i)=E^i . \quad (38)$$

However, the two particles will be propagated by different energies $\mathcal{E}_{\pm}(x_i)$ entering the function $\mathbf{G}(x_b,x_a|E)$ and hence they are assumed to pass through the system without any additional interference.

Thus the procedure is as follows: we excite a particle to level 2 at the position x_i with energy $E^i=U_2(x_i)$. This occurs with the probability $|a_2(x_i)|^2$. This particle is then split up on the two adiabatic levels with different energies. We then follow the propagation of each of these pieces through the system. The influence from the two intermediate paths is contained in the propagators (36) which are evaluated for the different energies, each one with its own weight determined by Eq. (37). The final probability of detecting the system on the bare level j is then given by

$$\Pi_j=\int_{x_0-\mathcal{D}}^{x_0+\mathcal{D}} dx_i\{|G_{j2}(\mathcal{E}_{-}(x_i))|^2\cos^2[\theta(x_i)/2] + |G_{j2}(\mathcal{E}_{+}(x_i))|^2\sin^2[\theta(x_i)/2]\} \times|a_2(x_i)|^2 , \quad (39)$$

where we have combined the results from Eqs. (7), (36), and (37). The integration is carried out over a finite integration domain $\mathcal{D}$ that surrounds the initial packet, but does not encroach on the crossings.

This ends our pseudoclassical description of the interferometric approach to double level crossings. By changing the tuning of the laser, we can vary the parameters of the functions in Eq. (39). This is the expression we will compare with the numerically obtained, and fully quantum-mechanical, results in the next section.

IV. COMPARISON OF NUMERICAL RESULTS

Figure 4 shows the spatially integrated probability Π_2 as a function of the detuning parameter Δ. The solid curve is obtained from a fully quantum-mechanical integration on a Cray computer. All the calculations cease above $\Delta\sim 9.1\times 10^5$ because beyond that point there are no level crossings. In that situation there is no effective coupling, and the packet remains in its original level. The positions of the level crossings as functions of Δ are shown in Fig. 5. Here we also see that if $\Delta\lesssim 5.0\times 10^5$ we cannot use our approach because the initial position of the wave packet is at $x_0=-3.79$. This happens at the lower end of Fig. 4 where the first crossing is approaching the position of the initial packet. This means that the packet develops very little kinetic energy up to the first crossing, so it passes over it slowly and adiabatically. As a result the packet is split so unequally between the levels that the fringes have very little visibility. The second crossing, being at a similar potential energy, is also nearly adiabatic resulting in very little overall transfer of probability after both the crossings.

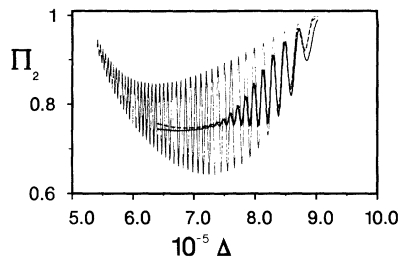

FIG. 4. In this figure we plot the final population Π_2 as a function of the detuning parameter Δ, but with other parameters the same as in Figs. 2 and 3. The solid curve shows the full quantum-mechanical result, which has been obtained numerically. The dashed curve shows the pseudoclassical calculations for the same parameters. The dotted curve shows the fringes from a single pseudoclassical calculation, before ensemble averaging and starting from the mean position of the packet ($x_0=-3.79$). This shows that the averaging process destroys many of the fringes, while leading to quite an accurate result. Disagreement occurs when the two crossings become close to each other or if the first crossing approaches the initial position of the packet (see Fig. 5).

The final value of Π_2 at the end of the motion shown in Figs. 3(a) and 3(b) is represented by a single point in Fig. 4 (when $\Delta=7.0\times 10^5$). It can be seen that this is close to the place where the oscillations in the solid curve start to develop for increasing Δ. And as Fig. 3 shows, the outgoing packets are just beginning to have diverging trajectories at this point, so it seems that there is some connection. Qualitatively this is because as Δ increases the two crossings come closer together, allowing a lesser interval for the development of a time difference in the emerging packets. If this difference is too great the interference is lost. However, the interpretation is different in terms of the time-independent states, or modes. To show this, we plot, as the dotted curve with many oscillations, the result from a single pseudoclassical calculation (where $x_i=x_0$), before averaging over x_i. It shows a full range of fringes as a function of Δ. So we see that the fringes are partially destroyed only after averaging; this is the result shown as the dashed curve which closely matches the direct integration of the Schrödinger equation. This loss of fringes means that only for lower values of Δ is the phase of the fringe pattern, before averaging, sensitive to the initial total energy $U_2(x_i)$.

The fit of the pseudoclassical calculation (dashed

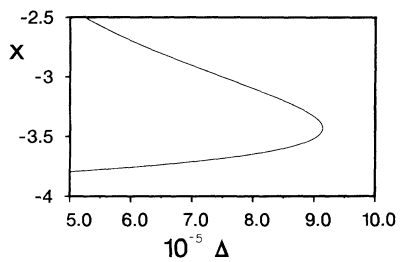

FIG. 5. We plot the position of the crossings as a function of Δ. The lower branch of the curve represents x_a and the upper branch represents x_b.

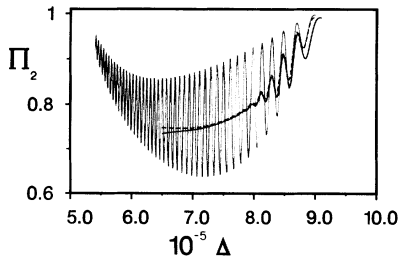

FIG. 6. Same as Fig. 4, but with $\sigma_0=0.02$ and $V=2.0\times10^4$.

curve) to the quantum calculation (solid curve) is very good, with the principal deviations occurring at the ends of the figure shown. The upper end (high Δ) shows bad agreement on the last fringe because this is where the two crossings approach each other prior to disappearing. The hypothesis of separate crossings breaks down as the coupling remains effective at creating non-adiabatic transitions between the crossings. For small couplings, progress could be made by considering a quadratic dependence of Eq. (28) on time [9].

In Fig. 6 we show what happens if we double the width of the initial wave packet. It is satisfying to see that the pseudoclassical calculation still gives a good agreement with the quantum-mechanical calculation, but the number of visible fringes has become reduced. In the wave-packet picture this is surprising because we expect that wider packets will have a greater possibility for more overlap in the final state; i.e., they will lead to more fringes. However, a wider initial wave packet also means that there is a greater range of energy in the packet, leading to diverging trajectories or greater incoherence during the x_i integration in the time-independent picture.

In Fig. 7 we return to the previous initial packet width of Fig. 4, but we reduce the coupling V. (This corresponds to turning down the intensity of the coupling laser in the physical system.) The population Π_2 shows a much greater swing (higher visibility) because of more equal splitting of the packets at the crossings. However, the number of visible fringes is not changed because this is controlled less by the coupling and more by the packet width and the shape of the potentials between the crossings.

V. CONCLUSIONS

We have considered the model in Fig. 1(a), where an electronic wave packet is created on a Born-Oppenheimer

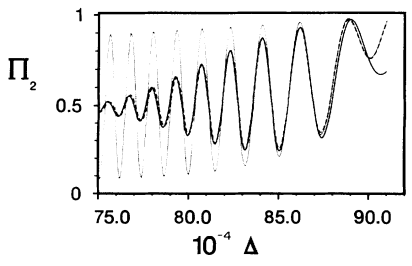

FIG. 7. Same as Fig. 4, but with $\sigma_0=0.01$ and $V=1.3\times10^4$.

state in a molecule. When this travels along the potential surface, it is mixed with another level by the action of a laser coupling. In this way the wave packet is split up, and later recombined. This leads to interference which has been considered the analogue of an optical interferometer.

We have used an energy decomposition of the initial state to follow the quantum-mechanical phases through the system, and we have found that the dependence of the outgoing wave packet on the laser detuning and the parameters of the potentials can be calculated with a simple semiclassical method based on WKB states and the Landau-Zener matching of wave functions across the level crossings. In obtaining an agreement we have used the wave functions corresponding to the adiabatic potentials. To show the necessity of this we exhibit in Fig. 8 the same results shown in Fig. 4, but without the unaveraged interference fringes. Instead, we have added the results obtained from the WKB wave functions on the bare potentials with the energy chosen as in Sec. III. As we can see, the main period of the interference fringes comes out correctly, but the overall agreement is poor. Thus we have found that the adiabatic levels must be used.

Observing the interference fringes experimentally, one may hope to determine the potential surfaces of the molecule. Often, there is some knowledge about one of them, i.e., the dissociating potential may have been probed by scattering or the bound one by vibrational spectroscopy. The interferometric observation can then be used to determine the other potential. Methods have been developed to extract potential data from WKB states by molecular physicists; e.g., the Rydberg, Klein, and Rees (RKR) method [10].

In our case the situation is complicated by the fact that the Landau-Zener phase will change when the level crossings are moved. Thus not only will the phase integral enter the problem, but also the crossing parameters with their dependence on potential slope and particle velocity. This complicates the picture and prevents a straightforward inversion of the interferometric data.

Using one laser for both level crossings will make the number of uncontrolled parameters very large as the two

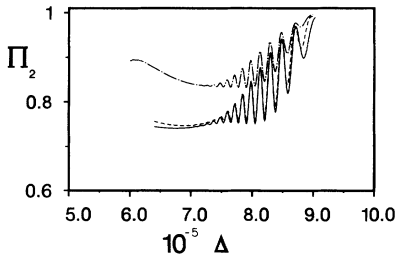

FIG. 8. The upper chained curve (short chain) shows what happens when we carry out the pseudoclassical calculation with the propagation part on the bare states (rather than the adiabatic states) between the crossings. There is a significant difference even though the positions of the fringes are similar to the correct calculation. As before, the solid and dashed curves show the quantum-mechanical result and the normal pseudoclassical results, respectively. The parameters are the same as in Fig. 4.

crossings differ greatly. The situation can be improved by the use of two lasers. We may then keep one crossing fixed with a preassigned splitting ratio (preferably close to 50% for each wave packet). By tuning the other laser we can move the second crossing and study the shape of the potentials around it. The main problem with the use of two lasers with different frequencies is the danger of having four crossings appearing. This will complicate the situation and care must be exercised if the packet is to traverse only two crossings. In special situations, one may be able to consider more complicated level configurations where a third level would be used as part of the interferometer. Thus some disadvantages could be avoided at the expense of additional difficulties in the interpretation of the experimental results.

In conclusion, we have suggested an interferometric arrangement inside a molecule. We have indicated that this may be used to acquire information about the molecular energy surfaces, but we have pointed out the technical difficulties in interpreting the resulting data. However, combined with other independent information about the molecule, this approach could offer valuable insight into, or confirmation of, the molecular spectra.

ACKNOWLEDGMENT

The authors wish to thank the Centre for Scientific Computing (CSC) at the Finnish State Computer Centre (VTKK) for access to the Cray X-MP EA supercomputer.

[1] See the forthcoming special issue of Appl. Phys. B.

[2] M. Gruebele and A. H. Zewail, Phys. Today **43** (5), 24 (1990).

[3] N. F. Scherer, R. J. Carlson, A. Matro, Mei Du, A. J. Ruggiero, V. Romero-Rochin, J. A. Cina, G. R. Fleming, and S. A. Rice, J. Chem. Phys. **95**, 1487 (1991).

[4] K.-A. Suominen, B. M. Garraway, and S. Stenholm, Phys. Rev. A **45**, 3060 (1992).

[5] B. M. Garraway, K.-A. Suominen, and S. Stenholm, in *Light Induced Kinetic Effects on Atoms, Ions and Molecules,* edited by L. Moi, S. Gozzini, C. Gabbianini, E. Arimondo, and F. Strumia (ETS Editrice, Pisa, 1991), p. 129.

[6] B. M. Garraway and S. Stenholm, Opt. Commun. **83**, 349 (1991).

[7] L. D. Landau, Phys. Z. Sowjetunion **2**, 46 (1932); C. Zener, Proc. R. Soc. London, Ser. A **137**, 696 (1932).

[8] A. P. Kazantsev, G. I. Surdutovich, and V. P. Yakovlev, *Mechanical Action of Light on Atoms* (World Scientific, Singapore, 1990), p. 41.

[9] K.-A. Suominen, Opt. Commun. (to be published).

[10] E. A. Mason and L. Monchick, Adv. Chem. Phys. **12**, 329 (1967); W. H. Miller, J. Chem. Phys. **54**, 4174 (1971); W. C. Stwalley, Contemp. Phys. **19**, 65 (1978).

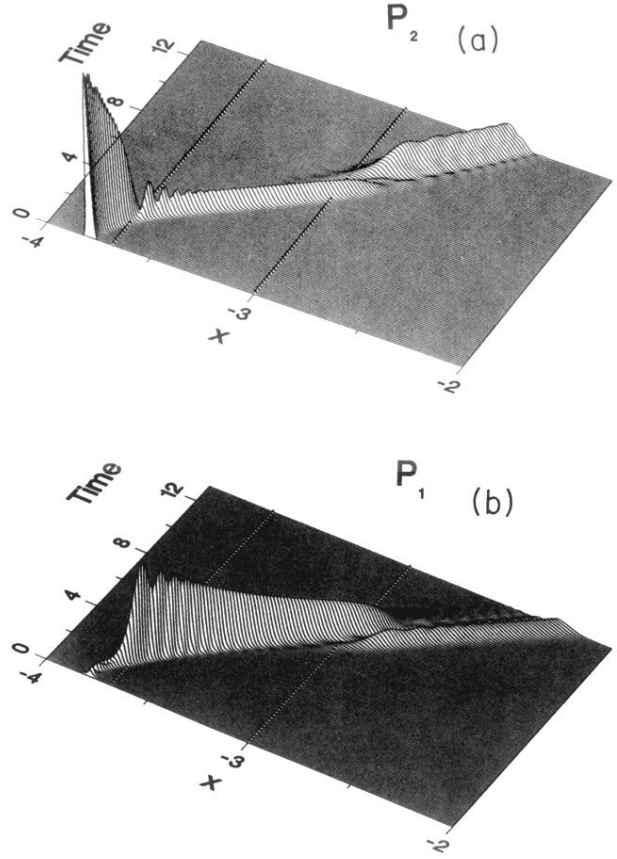

FIG. 3. This figure shows the wave-packet motion on the two levels as a function x and t. The probability density $P_2(x,t)$ is plotted in (a) and $P_1(x,t)$ is shown in (b). The initial position of the wave packet is $x_0=-3.79$, its width is $\sigma_0=0.01$, and the coupling is $V=2.0\times10^4$. Other parameters are the same as in Fig. 2.